Weeks-Long and Years-Long Slow Slip and Tectonic Tremor Episodes on the South Central Alaska Megathrust

Baptiste Rousset[1], Yuning Fu[2], Noel Bartlow[1], and Roland Bürgmann[1]

[1]Department of Earth and Planetary Science, University of California, Berkeley, Berkeley, CA, USA, [2]School of Earth, Environment and Society, Bowling Green State University, Bowling Green, OH, USA

Abstract We jointly investigate aseismic slip transients and tremor activity in south central Alaska. Near the eastern downdip edge of the M_w 9.2 1964 Prince Williams earthquake rupture, kinematic modeling of the $M_w = 7.6$ 2009–2013 slow slip event suggests cumulative transient slip of up to 55 cm. During this 5-year transient event, tectonic tremors were co-located with the inferred aseismic slip zone and occurred in weeks-long bursts of events. A short-term transient deformation event is observed in the GPS time series spanning a tremor burst in September 2010. The time-dependent slip modeling of this $M_w = 6.9$ subevent shows that it migrated along strike with tremor at speeds of ∼8 km/day and with slip rates of ∼3 mm/day. It released 9% of the 5-year transient event total moment in 1.4% of its duration. The decomposition of GPS time series relative to tremor times during the whole 5-year transient event shows that GPS site velocities were on average three to six times higher during tremor bursts than in between, suggesting that slip pulses are generally associated with tremor bursts. This inference is strengthened by the decomposition of the GPS time series after the 5-years-long deformation event, during which the plate interface is being loaded in between the short-duration events and slips at times of tremor bursts. The 5-years-long transient deformation event could either represent a cluster of short-term events or be the sum of short-term ETS events and a smooth long-term slip event located updip.

1. Introduction

Slow slip events (SSEs) lasting from days to years happen downdip of young and warm subduction seismogenic zones (Dragert et al., 2001; Schwartz & Rokosky, 2007), where increasing temperatures and pressures are responsible for the transition from seismic behavior to slow and stable deformation. SSEs recorded geodetically are frequently accompanied by noisy emergent seismic signals called tectonic tremors (Obara, 2002), thought to be clusters of low-frequency earthquakes (Shelly et al., 2007). When tremor and geodetically observed slip are occurring jointly, they are called episodic tremor and slip (ETS) events (Rogers & Dragert, 2003; Obara et al., 2004). The presence of high pore fluid pressure resulting from metamorphism dehydration reactions as inferred by V_p/V_s positive anomalies (Audet et al., 2009; Shelly et al., 2006) is invoked as a major factor to explain the occurrences of these slow slip phenomena.

In this study, we focus on analyzing simultaneously geodetic and seismic tremor observations in south central Alaska, where only independent studies of either phenomena have been carried out. At the eastern end of the Alaska-Aleutian subduction zone, the Pacific plate subducts at a rate of ∼5 cm/year beneath the North American plate (Figure 1). The accretion of oceanic terranes formed the Yakutat microplate located above the Pacific plate and limited by right-lateral transform faults, including the Fairweather-Queen Charlotte fault, to its eastern side. The subduction of this microplate appears to relate to a low slab dip angle (<5°), the presence of SSEs, tectonic tremors and low-frequency earthquakes, and a gap in the volcanic arc (Chuang et al., 2017; Eberhart-Phillips et al., 2006; Peterson & Christensen, 2009; Wech, 2016) (Figure 1). Receiver function analyses highlight a 3- to 5-km-thick low-velocity layer at the top of the subducting terrane that is interpreted as a zone of high pore fluid pressure, possibly due to fluid enriched sediments (Kim et al., 2014).

Years-long transient slip events have been recorded by continuous GPS position measurements below the lower and upper Cook Inlet, downdip of the seismic 800-km-long asperity that ruptured during the M_w 9.2 great 1964 earthquake (Christensen & Beck, 1994; Johnson et al., 1996). Below the upper Cook Inlet, a first event was observed soon after the installation of continuous GPS stations between 1998 and 2001 with an estimated moment magnitude M_w of 7.2 (Ohta et al., 2006). A second 5-years-long M_w 7.6 event occurred
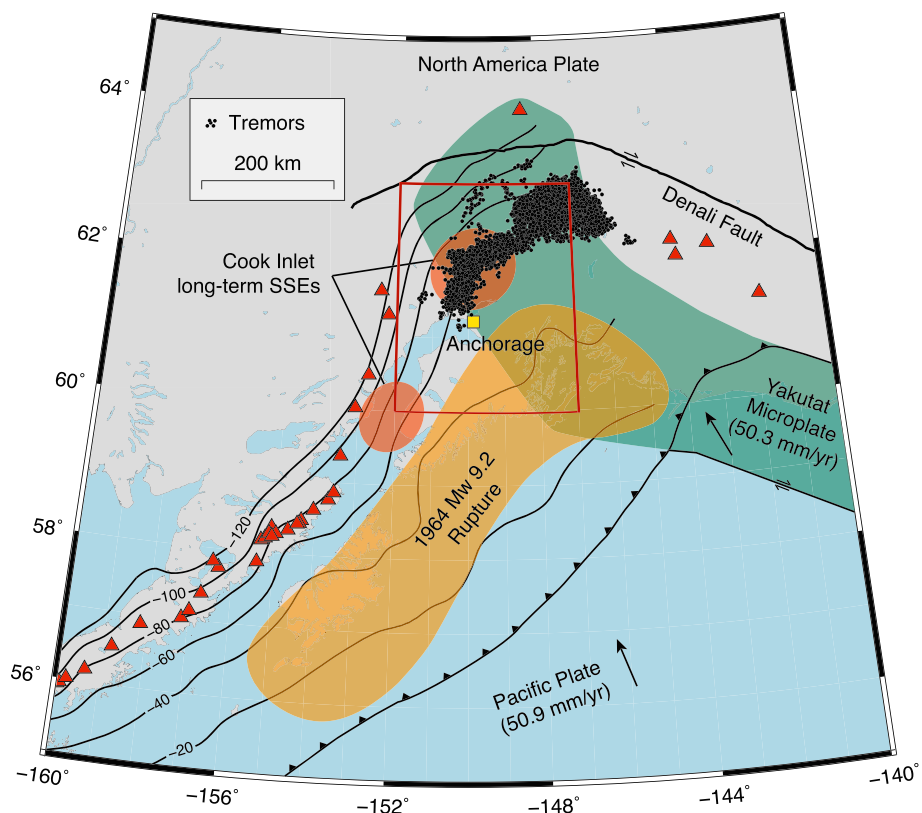
Figure 1. Tectonic setting of south central Alaska, where the Pacific plate subducts beneath the North American plate. At the eastern end of the Aleutian-Alaska subduction zone, the subducting Yakutat microplate is shown in green. Slab depth contours (Hayes et al., 2012) are indicated by the black thin lines. The right-lateral strike-slip Denali fault is shown by the thicker black line. The 1,000-km-long rupture area of the M_w 9.2 1964 earthquake is indicated by the yellow area (Christensen & Beck, 1994) and approximate contours for the geodetically observed years-long slow slip events by the red areas. The black dots indicate the tectonic tremor locations (Wech, 2016). Red triangles show major volcano locations. Note the gap associated with the width of the Yakutat microplate. The red contour is the close-up corresponding to Figure 2.

from 2009 to 2013 (Fu & Freymueller, 2013; Fu et al., 2015). Below the lower Cook Inlet, a smaller event of M_w 6.9 occurred from 2010 to 2011 (Wei et al., 2012). From their analysis of GPS campaign measurements, Li et al. (2016) suggest the occurrence of another 9-years-long event below the lower Cook Inlet that ended at the end of 2004 with a minimum M_w of 7.8.

Tectonic tremors have also been detected below the upper Cook Inlet (Wech, 2016). A significant increase in the tremor rate late 2012 is due to an improvement of the station coverage. Their horizontal extent appears to coincide well with the width of the Yakutat microplate subduction (Wech, 2016). While their depths are poorly constrained, six low-frequency earthquake families found within the tremor signals are located on the plate interface in the eastern tremor zone, at ∼60-km depth (Chuang et al., 2017). The tremor activity is continuous in the eastern tremor zone, and much more episodic in the west, at the location of observed SSEs. The tremors found during the 2009–2013 5-year transient event overlap with the maximum slip amplitude found by Fu and Freymueller (2013) and our study (Figure 2a). The source time function of this SSE derived from GPS observations has been suggested to be very smooth during the 5 years, with almost constant slip rates (Fu et al., 2015). However, the co-located tremor activity was very episodic during this time period (Figure 2c).

In order to better investigate the slow slip dynamics in south central Alaska, we conduct a joint analysis that reconciles both geodetic and tremor observations from 2008 to 2016, during which both data sets are available. We first revisit the static slip amplitude of the 2009–2013 SSE. We then analyze in detail a propagating tremor and slip episode in September 2010. And finally, by performing a decomposition of GPS time
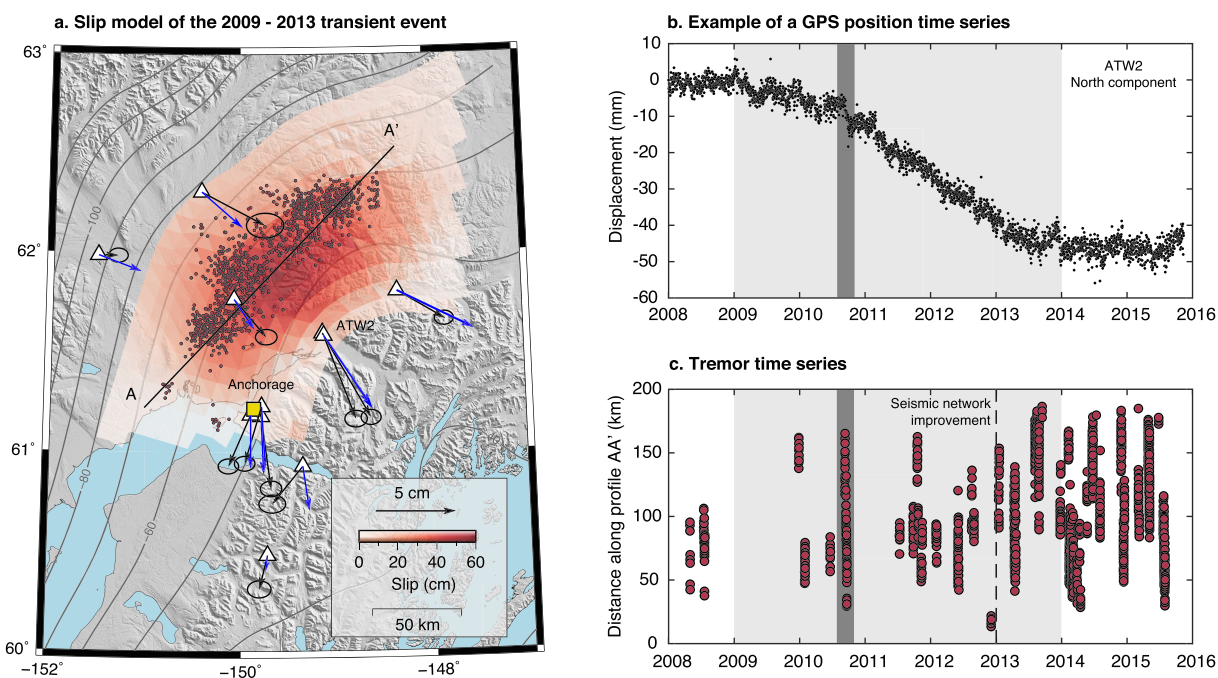
Figure 2. Geodetic and seismic observations of the 2009–2013 transient event. (a) Total static slip amplitude of the transient event and tremor locations from 2008 to 2016. GPS stations are indicated by white triangles. The total GPS-measured offset is shown by the black arrows tipped with 1-sigma confidence ellipses and the model prediction by the blue arrows. (b) North component of the position time series of GPS station ATW2 from 2008 to 2016. The light gray rectangle indicates the duration of the 5-year transient. The darker gray bar highlights the September 2010 subevent studied in details in Section 3.2. (c) Tremor time series projected along the profile AA′ shown in (a).

series, we assess the average surface displacement contributions during versus in between tremor episodes, finding that slip occurs predominantly during tremor bursts.

2. GPS Observations

In this study, we use position time series from 11 GPS stations processed as in Fu and Freymueller (2013) and Fu et al. (2015), in point positioning mode using GIPSY/OASIS version goa-5.0 developed by the Jet Propulsion Laboratory. Jet Propulsion Laboratory's reanalyzed orbit and clock products as well as IGS05 absolute antenna phase models are used. Ocean tidal loading effects are computed with ocean tide model TPXO7.0 (Egbert & Erofeeva, 2002), and loading deformation is computed in an Earth's center of mass reference frame (Fu et al., 2012). Individual daily solutions are then aligned with the ITRF2008 reference frame (Altamimi et al., 2011). Final GPS time series are referenced to the fixed North American plate using the plate model of Altamimi et al. (2012). Offsets due to local earthquakes or antenna changes are modeled by Heaviside functions at times of the offsets. Time series are then detrended from the best linear fits of data spanning interseismic periods outside of the 5-year transient deformation event, before 2009 and after 2013 (supporting information, Figure S1). We selected stations that have data at least 1 year before the start of the transient event in January 2009. We discarded three stations that have unusually large multi-year transient signals, particularly on the vertical component (AC15, AC20, and TLKA), which are likely due to local hydrological effects (Fu et al., 2012). Further analysis to assess how hydrology-related seasonal deformation can affect our results is described later in the text.

3. Modeling Long- and Short-Term Slow Slip Transient
3.1. Static Slip Inversion of the 2009–2013 Transient Event

The 2009–2013 transient event is clearly recorded by horizontal motions of 11 GPS stations, with surface displacement amplitudes of up to 50 mm on the north component at site ATW2, located in Palmer (Figure 2b). In order to model the total slip associated with this transient event, we discretized the subduction interface into triangular dislocation patches with ~10-km-long edges, following the 3-D geometry of the Slab1.0 model (Hayes et al., 2012). Green's functions, $\mathbf{G}$, relating unit slip on each patch to surface displacements

are computed for a homogeneous, isotropic, elastic half-space (Thomas, 1993). The slip rake angle is computed independently for each patch in the plate convergence direction, considering the Euler pole between the Pacific plate and the North American plate ($-48.89°$N, $108.29°$E) from the MORVEL plate motion model (DeMets et al., 2010). We then solve for the slip on each patch, $\mathbf{m}$, using the general least squares solution (Tarantola, 2005):

$$\mathbf{m} = \mathbf{m}_0 + \mathbf{C}_m \mathbf{G}^t (\mathbf{G} \mathbf{C}_m \mathbf{G}^t + \mathbf{C}_d)^{-1} (\mathbf{d} - \mathbf{G} \mathbf{m}_0),\tag{1}$$

where $\mathbf{m}_0$ is an a priori model (a null vector in this case). $\mathbf{d}$ includes the static offsets for the north and east components of the 11 stations used. $\mathbf{C}_d$ is a diagonal matrix including uncertainty variances (σ_d^2) associated with the transient station offsets, where σ_d is two times the time series standard deviation. The covariance between model parameters $\mathbf{C}_m$ is computed as (e.g., Nocquet et al., 2014; Radiguet et al., 2011; Rousset et al., 2016):

$$\mathbf{C}_m = \left(\frac{\sigma_m \lambda}{\lambda_0} \right)^2 \exp\left(\frac{\mathbf{x}}{\lambda} \right),\tag{2}$$

where σ_m is an a priori standard deviation on the model parameters fixed to 0.5 m. λ_0 is a scaling factor fixed at 10 km, λ is the correlation length, and $\mathbf{x}$ is a vector with distances between pairs of patch centroids. In the model that we present in Figure 2, $\lambda = 50$ km. Such a smoothing is a good compromise between rough models that overfit the data and very smoothed models, as estimated by the L-curve criterion (Radiguet et al., 2011). The inverted slip area is consistent with the distribution of tremors (Figure 2). The updip limit of the slip area coincides with the transition between the locked seismogenic zone and the creeping zone as estimated by Li et al. (2016). This transient slip event has a total moment of 2.28×10^{20} N·m (for a shear modulus of 50 GPa), which corresponds to an equivalent moment magnitude $M_w = 7.6$. Estimates of the shear modulus derived from seismic velocities in this region vary from 30 GPa at 10-km depths to 70 GPa at 60-km depths (Freed et al., 2006). We thus selected an average value of 50 GPa, as in Ohta et al. (2006) and Fu et al. (2015). In comparison with previous published models (Fu & Freymueller, 2013; Fu et al., 2015), our inferred slip pattern is more compact, with a maximum amplitude of $\sim$55 cm. However, the moment magnitude of our model is similar to that estimated by Fu and Freymueller (2013, $M_w = 7.5$) and by Fu et al. (2015, $M_w = 7.6$). We did not use the GPS vertical components since the transient offset is uncertain at most GPS sites. It seems however clear at site ATW2, with an uplift of $\sim$50 mm (Figure S1). This signal implies that most of the transient slip is located north of this station, which is in agreement with the model presented in Figure 2.

3.2. The September 2010 Tremor and Slip Pulse

While the GPS position time series mainly present the transient event from 2009 to 2013 (Figure 2b), the tremor activity exhibits shorter-term episodic bursts during this 5-year period (Figure 2c). By visually inspecting GPS time series windows around each tremor burst, we identified a clear short-term transient event in September 2010, with surface displacements of up to 8 mm, comparable to the surface deformation amplitudes of the largest Cascadia SSEs (Bartlow et al., 2011). The associated 15-day tremor burst started on September 10 and propagated southwest at a speed of about 8 km/day (Figure 3). During this time, the transient event is recorded by five GPS stations, mainly on the north component. In order to model the time-dependent slip during this ETS, we use the network inversion filter (NIF) (e.g., Bartlow et al., 2011; McGuire & Segall, 2003; Segall & Matthews, 1997). We modeled 89 days of GPS position times series as

$$\mathbf{x}(t) = \mathbf{x}(t_0) + \mathbf{G}\mathbf{m}(t - t_0) + F\mathbf{f}(t) + \mathbf{L}(t - t_0) + \epsilon,\tag{3}$$

where $\mathbf{x}(t)$ is the modeled position at each time step and $\mathbf{x}(t_0)$ is the initial position. $\mathbf{G}$ and $\mathbf{m}$ are Green's functions and the slip in the fixed-rake plate convergence direction, as described in Section 3.1 for the inversion of the static offsets of the 5-year transient. $F\mathbf{f}(t)$ represents reference frame errors, where F is a matrix including a whole network translation and $\mathbf{f}(t)$ is a time-dependent scalar reference frame wobble noise term. $\mathbf{L}$ models the local benchmark motion as a Brownian random walk with scale parameter $\tau = 1$ mm/year$^{1/2}$ and ϵ is a residual error assumed to be white noise. The NIF estimates the slip and the slip rate at each time step through a recursive Kalman filter (refer to McGuire & Segall (2003); Segall & Matthews (1997) for a complete description of the method). The slip is spatially smoothed at each temporal iteration by minimizing its second derivative (Laplacian) between adjacent fault patches. We used temporal hyperparameter
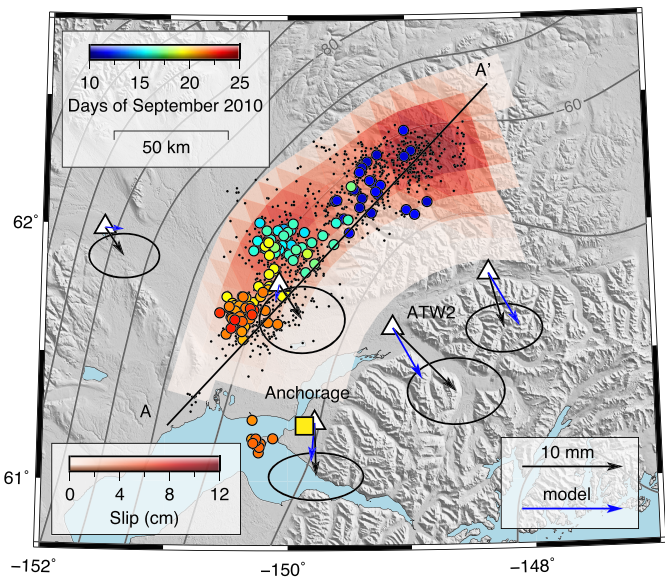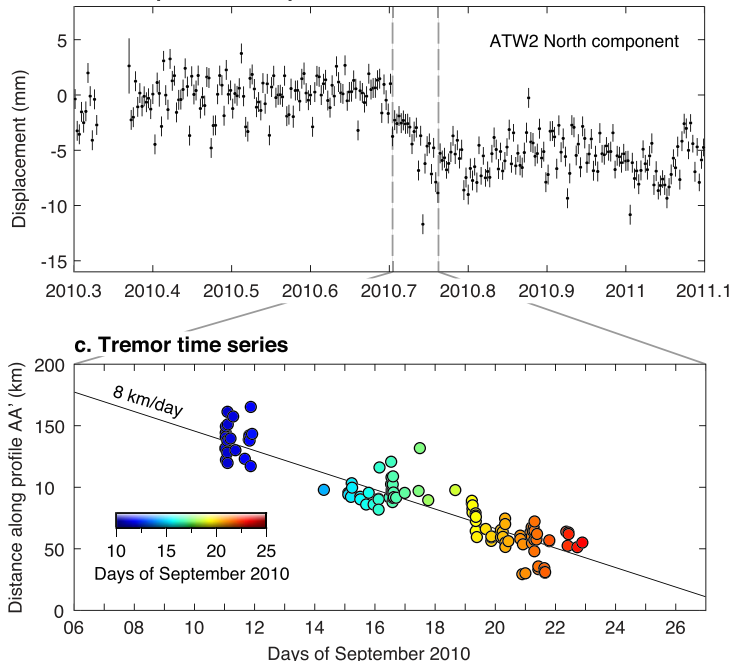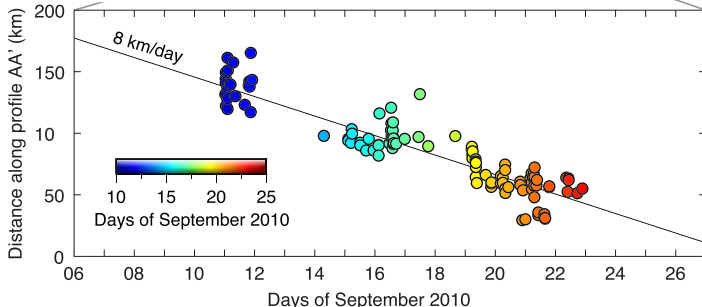
Figure 3. September 2010 slip and tremor episode. (a) Cumulative slip and tremors. The black arrows indicate the observed static offsets tipped with 1-sigma confidence ellipses and the blue arrows the model predictions. Tremors are colorcoded by days of September 2010. Black dots indicate tremor locations outside September 2010. (b) North component of the GPS time series of ATW2. (c) September 2010 tremor activity projected along the profile AA′ shown in (a). The 8 km/day propagation speed is indicated.

$\alpha = 60$ and spatial hyperparameter $\gamma = 1e^{-3}$. Similar values have been used for the modeling of SSEs of similar size and duration in Cascadia (Bartlow et al., 2011), and the temporal fit to the GPS time series is good for the timescale of the month-long transient event.

The maximum slip amplitude is ~10 cm and is co-located with the tremor activity (Figure 3). During this 27-day event, the slip corresponds to about 20% of the total slip during the 5 years at similar locations. The moment released by the ETS is 2.01×10^{19} N·m, which corresponds to an equivalent moment magnitude of 6.9 (with an assumed shear modulus of 50 GPa). During this September 2010 event, 9% of the 5-year transient event total moment was released in 1.4% of its duration, which means that the slip rate was 6.4 times higher than a slip rate considered as constant during the 5 years.

The time-dependent slip estimated from this analysis shows that the slip initiates to the northeast on September 2 and starts to propagate to the southwest around September 8, in the same direction as the tremors. During the second phase of the transient event, the whole slip area is activated with slip rates of about 0.3 cm/day and vanishes around September 29 (Figure 4). While this analysis could suggest that the propagating slip front precedes the tremor activity, this question is not resolvable with the actual data. The slip propagation is mainly constrained by the onsets of the transient on the north components of stations AC11, ATW2, and ZAN1 that are located on a parallel line to the slip propagation. However, the initiation of the slip likely appears in the model before it actually occurred as a result of the backwards temporal smoothing used in the NIF, as shown in Bartlow et al. (2011). Moreover, before 2013, the seismic network being quite sparse, only the most energetic tremors were recorded. Less energetic tremors are thus likely to have occurred before the ones presented in Figure 4.

3.3. Decomposition of GPS Position Time Series Relative to Tremor Occurrences

The detailed analysis of an individual ETS event is possible only for the September 2010 event, GPS offsets during other tremor burst periods being less obvious. A few other transients are present at times without tremors, which could either be tectonic since the tremor catalog is incomplete or of local non-tectonic origin. In order to do a more global analysis of offsets associated with tremor periods for the whole 5-year transient event, we realized a decomposition of the GPS time series based on the tremor times, similar to the one
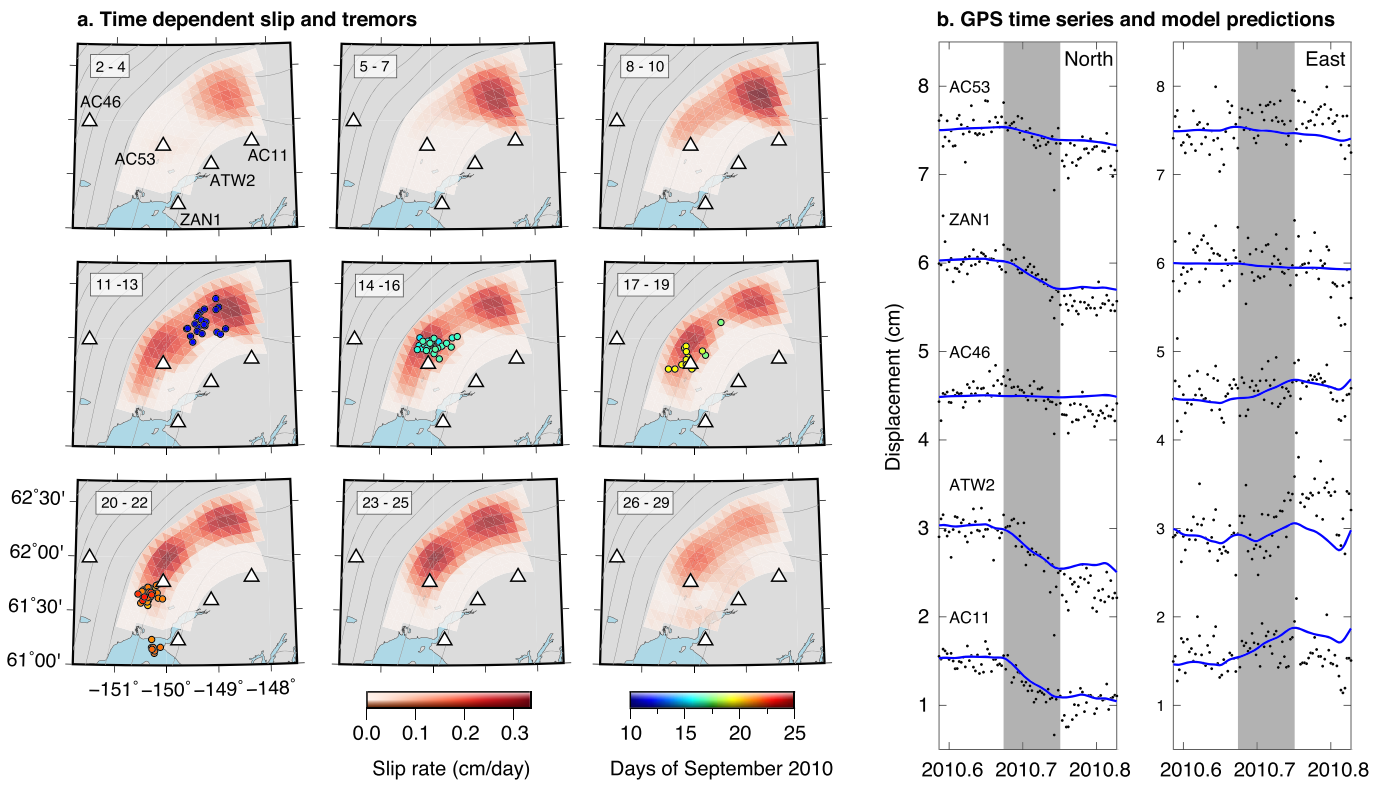
Figure 4. Time-dependent slip as estimated by the network inversion filter. (a) Each panel represents averaged slip rate over 3-day-long time periods inverted from GPS time series. The days of September 2010 for each time periods are indicated at the top-left corners of each panel. Tremors are color coded by days of September. The white triangles indicate the GPS stations. (b) GPS position time series (black dots) and model prediction (blue lines) for the north and east components. The gray areas indicate the duration of the transient event presented in (a).

performed by Frank et al. (2018). We did the decomposition for both during the 2009–2013 transient event and the subsequent period (from 2014 to 2016) for reference.

We assembled the daily-number-of-tremor time series in 18 clusters during the 5-year transient event and 13 in the following years, with minimum inter-cluster duration of 22 days (Figure S2). For each cluster, we estimated the associated displacement in the GPS time series by computing the difference between average
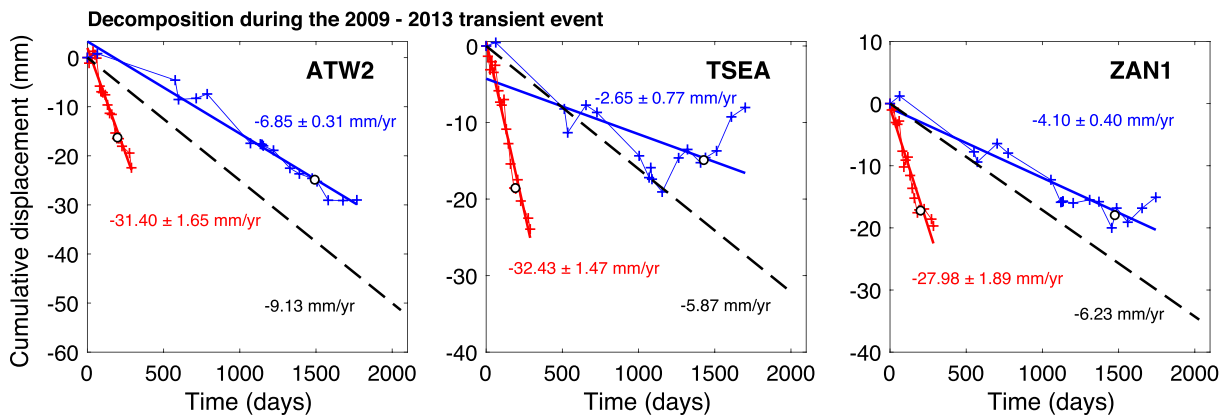
Figure 5. Decomposition of the GPS time series during the 2009–2013 transient event at GPS stations ATW2, TSEA, and ZAN1. The red and blue curves indicate the cumulative offsets during tremor and inter-tremor periods, respectively. White circles on curves indicate the time of seismic network improvements, after which a larger number of tremors have been detected. Labels indicate average velocities and their 1-sigma uncertainties. The dashed black lines show the average velocities during the 5-year duration of the transient event.
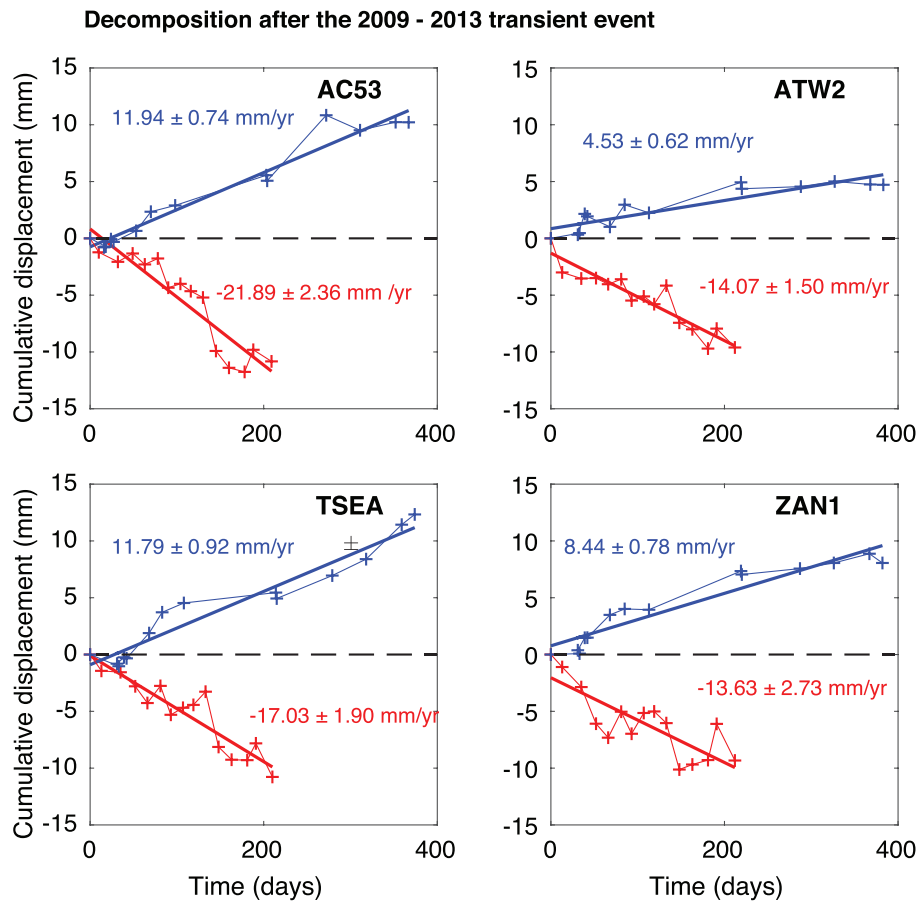
Figure 6. Decomposition of the GPS time series after the 2009–2013 transient event at GPS stations AC53, ATW2, TSEA, and ZAN1. As in Figure 5, red and blue curves indicate the cumulative offsets respectively during tremor and inter-tremor periods. Average velocities and their uncertainties are shown.

positions after and before each cluster over time windows of duration ΔT. We maximized ΔT ($\Delta T = 10$ days) so that $2\Delta T$ is still less than the minimum inter-cluster duration.

We then assembled the offsets for each tremor cluster in order to obtain time series of cumulative displacement associated with tremor and inter-tremor periods and perform linear fits to these time series to obtain a velocity estimates (Figures 5 and 6). Given that we used a window of duration ΔT to average the positions before and after each cluster, the duration associated with each tremor cluster is augmented by ΔT.

In order to quantify the robustness of these decompositions with regard to background noise levels, we removed the tremor periods from the GPS time series and performed decompositions by randomly sampling the same number of time periods with identical durations as the tremor clusters. We performed these decompositions for each component of all 11 GPS time series 10,000 times and assumed that the decomposition is robust if the average velocity obtained for the real tremor periods is more than 3σ from the mean of velocities obtained with the random decompositions associated with noise (Figures S3 and S4). The decompositions are found to be robust for the north component of three stations during the 5-year transient event, and the north component of four stations for the period following the 5-year event (Figures 5 and 6). No east components are determined to be robust, mainly because they are less sensitive to slip on the subduction interface, and their noise level is also higher than the north component. Also, potential seasonal signals in the GPS time series could bias the decompositions in the case of seasonally modulated tremor. To evaluate this possibility, we have computed the average number of days with tremors by month (Figure S5). This metric shows no apparent seasonality, tremors tend to happen randomly throughout the year. Thus, the decompositions seem not affected by seasonally modulated tremors.

During the 5-year transient event, the velocities are systematically higher during the tremor periods compared to the inter-tremor periods (Figure 5) and are 3.4 to 5.5 times higher than the averaged velocities over the 5 years. For the period after the 5-year transient event, the reference is flat, since the GPS time series have been detrended (Figure 6). The cumulative displacement associated with the tremor periods is systematically to the south, while the cumulative displacement during the inter-tremor periods is going north. In the context of the Alaska subduction zone, a displacement towards the north is consistent with tectonic loading due to increased locking of the subduction interface, while a displacement towards the south indicates tectonic release related to transient slow slips or reduced locking.

4. Discussion

4.1. Slip Dynamics in South Central Alaska

The GPS position time series in south central Alaska are dominated by a 5-year transient deformation event that can be modeled as a M_w 7.6 SSE on the subduction thrust with slip of up to 55 cm, co-located with tectonic tremors. The tremor activity during these 5 years and afterwards consists of shorter duration, day- to weeks-long bursts. In September 2010, a 3-weeks-long transient event associated with a tremor burst is well recorded by five GPS stations. It corresponds to an M_w 6.9 SSE, propagating along strike to the southwest with slip rates of about 0.3 cm/day. The accompanying tremors are migrating at a speed of 8 km/day. While this subevent is the only one clearly recorded by the GPS stations, the decomposition of GPS time series during the whole 5-year transient event shows that on average, the southward displacement rate, and thus the associated slip rate, is systematically higher by a factor of 3 to 6 during tremor periods than a constant slip rate over the 5 years. Moreover, the decomposition of the time series in the years following the 5-year event shows that the subduction interface is being loaded in between tremor bursts (GPS stations moving north), and sliding in SSEs during tremor bursts, releasing a fraction of the accumulated stress (GPS stations moving south). A similar observation is made in Cascadia and in Mexico, where decomposed GPS time series during apparent steady-state periods, in between clear transient events, show that slip seems to always occur in association with small tremor bursts alternating with loading periods (Frank, 2016).

The September 2010 ETS event and GPS decomposition during and after the 5-year transient event clearly show that short-lasting transient SSEs associated with tremor bursts are happening constantly (Figure 7a). The difference of velocities between the tremor periods and inter-tremor periods corresponds to the surface deformation associated with short-lasting SSEs (Table S1). These differences are very similar for the north component of GPS sites ATW2, TSEA, and ZAN1 during the 5-year transient and during the subsequent period, suggesting that the short-lasting ETS always occur at the same location. To explain the presence of the 5-year transient deformation event, we propose two end-member models (Figure 7b). A cluster of short-term ETS events (Figure 7b1) with more frequent and/or more energetic events would produce a long-term transient event in the GPS time series, as suggested for Mexico's 2006 6-month-long $M_w = 7.5$ transient slip event by Frank et al. (2018). The other end-member model suggests that the short-term ETS events behave in a similar fashion with the addition of a smooth 5-year SSE, likely away from and slightly updip of the short-term ETS events (Figure 7b2). With the decomposed GPS velocities, we cannot reliably locate a separate long-term SSE that would correspond to the blue velocities on Figure 5, given that the decomposition is robust only for the north component of three stations. However, we suggest that if a spatially distinct long-term SSE occurred, it should be located updip of the ETS events based on observations at other subduction zones. Indeed, an updip segmentation of SSEs with short-term events downdip and long-term events updip is observed both in Nankai (Nishimura et al., 2013; Takagi et al., 2019) and in Mexico (Frank et al., 2015; Rousset et al., 2017). Also, clusters of tremors are observed to have increased durations and recurrence intervals from downdip to updip in Nankai (Obara, 2011), Cascadia (Wech & Creager, 2011) and Mexico (Frank et al., 2015).

The GPS decomposition is not complete during the 5-year transient event, that is, GPS stations are still moving south during the inter-tremor periods. This observation tends to favor the model b2 in which GPS time series record the superposition of both short-term ETS and a long-term aseismic SSE. However, this interpretation has to be considered in light of the fact that before 2013 the seismic network was sparse, and thus, it is likely that many events were missed (Wech, 2016). A more complete catalog would likely improve the decomposition and might demonstrate the absence of an independent long-lasting SSE without tremor. Since the improvement of the seismic network occurred early 2013, about a year before the end of the long-term transient event, we can look in more detail at that last year. During this year, the inter-tremor
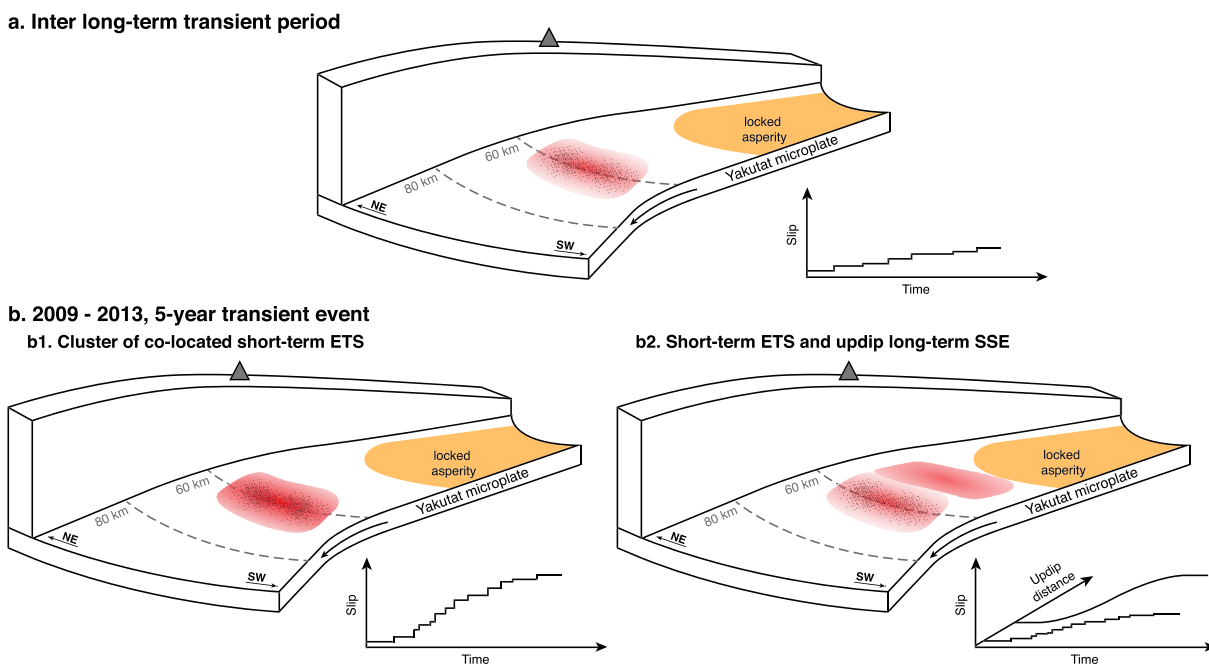
Figure 7. Sketch of the tremor and slip dynamics in south central Alaska. (a) Short-lasting ETS in between long-term transient events are occurring continuously. (b) Two end-member models for the 2009–2013 transient event. (b1) Clusters of short-term ETS with more frequent and/or more energetic short-term transient events produce accelerated surface deformation during the long-term transient. (b2) Continuous short-term ETS activity and updip long-term SSE combine to produce transient event. The slip as a function of time plots shows the slip on the red patches, which correspond to SSE locations. The orange patches indicate the eastern end of the seismic asperity that ruptured during the 1964 M_w 9.2 earthquake. The gray triangles indicate a GPS station that records the surface deformation due to varying slip rates below.

velocities are either neutral or moving north at the three stations (Figure 5). This is potentially in favor of model b1, suggesting an absence of aseismic SSE slip in between tremor bursts. But given the low number of tremor clusters during only 1 year, the associated velocities are poorly constrained.

4.2. Comparison With Other Slow Slip Phenomena Around the World

The association of short- and long-lasting transient slip events at a given subduction zone has been documented in the Nankai (Obara, 2011), Mexico (Frank et al., 2015; Rousset et al., 2017), and New Zealand (Bartlow et al., 2014; Wallace et al., 2012) subduction zones. In both Nankai (e.g., Obara & Kato, 2016) and Mexico (Frank et al., 2015; Rousset et al., 2017), short-term SSEs are co-located with tremor activity, and long-term SSEs are located updip of the tremor zone. In New Zealand, SSE segmentation is more complex, associated with lateral depth variations of the brittle to ductile transition. Short-term SSEs are located at shallower depths, where the transition is located at about 10-km depth, while the long-term ones are located at about 40-km depth (Wallace et al., 2012). The joint GPS and tremor analysis in our study shows that short-term SSEs in Alaska are co-located with tremors at about 60-km depth. However, the location of the long-term transient activity remains uncertain, either co-located with tremors or partly updip as discussed in the previous section.

Short-term ETS propagating along strike have been documented in Cascadia (Bartlow et al., 2011; Gomberg et al., 2010) and Nankai (Obara & Sekine, 2009). The September 2010 ETS event we discovered in Alaska has comparable along strike tremor migration speeds of ~8 km/day (Obara, 2002; Wech & Bartlow, 2014) and slip rates of ~0.3 cm/day (Bartlow et al., 2011; Hirose & Obara, 2010). Its moment magnitude ($M_w = 6.9$) with a rupture length of ~100 km is equivalent to the largest events in Cascadia (Bartlow et al., 2011) that ruptured 300-km-long asperities. Nankai ETS have lower M_w, ranging from 5.8 to 6.2, and ruptured about 50-km-long fault portions (Nishimura et al., 2013; Sekine et al., 2010). The relationship between fault area and moment predicts a stress drop of about 37 kPa for this transient event, which falls within the range of 10–200 kPa found for Cascadia SSEs (e.g., Bartlow et al., 2011). A feature distinguishing Alaska ETS from those in both Cascadia and Nankai is their depth of ~60 km (Chuang et al., 2017; Fu & Freymueller, 2013; Wech, 2016), whereas ETS in Cascadia and Nankai are found at ~40-km depth. This depth difference could in part be explained by a slightly colder slab in Alaska (Kirby et al., 1996).

AGU
100
ADVANCING EARTH
AND SPACE SCIENCE

Journal of Geophysical Research: Solid Earth

10.1029/2019JB018724

The striking similarities between all these propagating ETS events, particularly their along strike migration speeds and slip rates probably indicates similar underlying physical processes. Different mechanisms have been suggested to explain SSEs. In the framework of rate and state friction laws, slow transient events nucleate in a weakly slip weakening regime, close to velocity neutral, and with very low effective normal stress due to high pore pressure (Liu & Rice, 2005, 2007). Additional stabilization mechanisms at the transient slip onset such as dilatant strengthening have been suggested to quench instabilities (Segall et al., 2010).

Evidence of high pore fluid pressure related to metamorphic dehydration reactions comes from high V_p/V_s anomalies within the oceanic crust at locations of SSEs, in both Nankai (Shelly et al., 2006) and Cascadia (Audet et al., 2009). In Alaska, V_p/V_s anomalies are not that pronounced in published studies with values of about 2.0 for the low-velocity zone (e.g., Li et al., 2018). However, independent P and S mode scattered wave images suggest that the low-velocity zone associated with the subducting Yakutat microplate thins by ∼5 km at tremor depth, possibly indicating a velocity increase due to eclogitization of the upper crust (Rondenay et al., 2010). Also, a large amount of fluid being released is supported by high S-wave attenuation in Abers et al.'s (2006) tomography model. Moreover, tremors and LFEs are located in a region with a lack of nearby intraslab seismicity, compared to updip and downdip activity (Chuang et al., 2017). The large volume of fluids being released at tremor depths, associated with the low dip angle of the Yakutat microplate, could be an explanation for the absence of partial melt production and the Denali gap in arc volcanism (Chuang et al., 2017).

5. Conclusions

GPS position time series in south central Alaska are dominated by a 2009–2013 SSE on the deep subduction thrust, downdip of the 1964 M_w 9.2 Prince Williams earthquake rupture zone. However, the joint analysis of GPS time series and tectonic tremors reveals a more complex temporal slip dynamics. Tremor activity during this 5-year transient is concentrated in day- to weeks-long bursts of events. We document that both tremor and slip during a 1-month M_w 6.9 subevent in September 2010 migrated along strike at a rate of ∼8 km/day, with slip rates of ∼3 mm/day over a distance of ∼ 100 km. During this episode, 9% of the 5-year transient event's total moment is released in 1.4% of its duration, showing that slip rates are highly variable during the long-term transient. The decomposition of GPS time series relative to tremor times during the 5-year transient shows that southward surface displacement rates during tremor bursts are three to six times higher than considering a constant slip rate over the 5 years, demonstrating that slip pulses have a tendency to mostly occur during tremor. The decomposition of GPS time series during the years following the 5-year transient event strengthens this conclusion, showing that the subduction interface at ETS locations slips during tremor bursts and is being loaded between them. The exact nature of the 5-year transient remains unclear. This long-term transient could either be a cluster of short-term ETS events or it could reflect the combination of short-term ETS and a long-lasting aseismic slip event updip of the tremor zone. Further analysis during the next long-lasting transient events, with improved tremor detection and denser GPS network could help resolve this question.

References

Abers, G. A., van Keken, P. E., Kneller, E. A., Ferris, A., & Stachnik, J. C. (2006). The thermal structure of subduction zones constrained by seismic imaging: Implications for slab dehydration and wedge flow. *Earth and Planetary Science Letters*, *241*(3-4), 387–397.

Altamimi, Z., Collilieux, X., & Métivier, L. (2011). ITRF2008: An improved solution of the international terrestrial reference frame. *Journal of Geodesy*, *85*(8), 457–473.

Altamimi, Z., Métivier, L., & Collilieux, X. (2012). ITRF2008 plate motion model. *Journal of geophysical research*, *117*, B07402. https://doi.org/10.1029/2011JB008930

Audet, P., Bostock, M. G., Christensen, N. I., & Peacock, S. M. (2009). Seismic evidence for overpressured subducted oceanic crust and megathrust fault sealing. *Nature*, *457*(7225), 76.

Bartlow, N. M., Miyazaki, S., Bradley, A. M., & Segall, P. (2011). Space-time correlation of slip and tremor during the 2009 Cascadia slow slip event. *Geophysical Research Letters*, *38*, L18309. https://doi.org/10.1029/2011GL048714

Bartlow, N. M., Wallace, L. M., Beavan, R. J., Bannister, S., & Segall, P. (2014). Time-dependent modeling of slow slip events and associated seismicity and tremor at the Hikurangi subduction zone, New Zealand. *Journal of Geophysical Research: Solid Earth*, *119*, 734–753. https://doi.org/10.1002/2013JB010609

Christensen, D. H., & Beck, S. L. (1994). The rupture process and tectonic implications of the great 1964 Prince William Sound earthquake. *Pure and Applied Geophysics*, *142*(1), 29–53.

Chuang, L., Bostock, M., Wech, A., & Plourde, A. (2017). Plateau subduction, intraslab seismicity, and the Denali (Alaska) volcanic gap. *Geology*, *45*(7), 647–650.

DeMets, C., Gordon, R. G., & Argus, D. F. (2010). Geologically current plate motions. *Geophysical Journal International*, *181*(1), 1–80.

Dragert, H., Wang, K., & James, T. S. (2001). A silent slip event on the deeper Cascadia subduction interface. *Science*, *292*(5521), 1525–1528.

Eberhart-Phillips, D., Christensen, D. H., Brocher, T. M., Hansen, R., Ruppert, N. A., Haeussler, P. J., & Abers, G. A. (2006). Imaging the transition from Aleutian subduction to Yakutat collision in central Alaska, with local earthquakes and active source data. *Journal of Geophysical Research*, *111*, B11303. https://doi.org/10.1029/2005JB004240

Egbert, G. D., & Erofeeva, S. Y. (2002). Efficient inverse modeling of barotropic ocean tides. *Journal of Atmospheric and Oceanic Technology*, *19*(2), 183–204.

Frank, W. B. (2016). Slow slip hidden in the noise: The intermittence of tectonic release. *Geophysical Research Letters*, *43*, 10,125–10,133. https://doi.org/10.1002/2016GL069537

Frank, W. B., Radiguet, M., Rousset, B., Shapiro, N. M., Husker, A. L., Kostoglodov, V., et al. (2015). Uncovering the geodetic signature of silent slip through repeating earthquakes. *Geophysical Research Letters*, *42*, 2774–2779. https://doi.org/10.1002/2015GL063685

Frank, W. B., Rousset, B., Lasserre, C., & Campillo, M. (2018). Revealing the cluster of slow transients behind a large slow slip event. *Science Advances*, *4*(5), eaat0661.

Frank, W. B., Shapiro, N. M., Husker, A. L., Kostoglodov, V., Bhat, H. S., & Campillo, M. (2015). Along-fault pore-pressure evolution during a slow-slip event in Guerrero, Mexico. *Earth and Planetary Science Letters*, *413*, 135–143.

Freed, A. M., Bürgmann, R., Calais, E., Freymueller, J., & Hreinsdóttir, S. (2006). Implications of deformation following the 2002 Denali, Alaska, earthquake for postseismic relaxation processes and lithospheric rheology. *Journal of Geophysical Research*, *111*, B01401. https://doi.org/10.1029/2005JB003894

Fu, Y., & Freymueller, J. T. (2013). Repeated large slow slip events at the southcentral Alaska subduction zone. *Earth and Planetary Science Letters*, *375*, 303–311.

Fu, Y., Freymueller, J. T., & Jensen, T. (2012). Seasonal hydrological loading in southern Alaska observed by GPS and GRACE. *Geophysical Research Letters*, *39*, L15310. https://doi.org/10.1029/2012GL052453

Fu, Y., Liu, Z., & Freymueller, J. T. (2015). Spatiotemporal variations of the slow slip event between 2008 and 2013 in the southcentral Alaska subduction zone. *Geochemistry, Geophysics, Geosystems*, *16*, 2450–2461. https://doi.org/10.1002/2015GC005904

Gomberg, J., 2007, Cascadia, & Group, B. W. (2010). Slow-slip phenomena in Cascadia from 2007 and beyond: A review. *Bulletin*, *122*(7–8), 963–978.

Hayes, G. P., Wald, D. J., & Johnson, R. L. (2012). Slab1.0: A three-dimensional model of global subduction zone geometries. *Journal of Geophysical Research*, *117*, B01302. https://doi.org/10.1029/2011JB008524

Hirose, H., & Obara, K. (2010). Recurrence behavior of short-term slow slip and correlated nonvolcanic tremor episodes in western Shikoku, southwest Japan. *Journal of Geophysical Research*, *115*, B00A21. https://doi.org/10.1029/2008JB006050

Johnson, J. M., Satake, K., Holdahl, S. R., & Sauber, J. (1996). The 1964 Prince William Sound earthquake: Joint inversion of tsunami and geodetic data. *Journal of Geophysical Research*, *101*(B1), 523–532.

Kim, Y., Abers, G. A., Li, J., Christensen, D., Calkins, J., & Rondenay, S. (2014). Alaska Megathrust 2: Imaging the megathrust zone and Yakutat/Pacific Plate interface in the Alaska subduction zone. *Journal of Geophysical Research: Solid Earth*, *119*, 1924–1941. https://doi.org/10.1002/2013JB010581

Kirby, S., Engdahl, R. E., & Denlinger, R. (1996). Intermediate-depth intraslab earthquakes and arc volcanism as physical expressions of crustal and uppermost mantle metamorphism in subducting slabs. *Subduction: Top to bottom*, *96*, 195–214.

Li, S., Freymueller, J., & McCaffrey, R. (2016). Slow slip events and time-dependent variations in locking beneath Lower Cook Inlet of the Alaska-Aleutian subduction zone. *Journal of Geophysical Research: Solid Earth*, *121*, 1060–1079. https://doi.org/10.1002/2015JB012491

Li, H., Wei, M., Li, D., Liu, Y., Kim, Y., & Zhou, S. (2018). Segmentation of slow slip events in south central Alaska possibly controlled by a subducted oceanic plateau. *Journal of Geophysical Research: Solid Earth*, *123*, 418–436. https://doi.org/10.1002/2017JB014911

Liu, Y., & Rice, J. R. (2005). Aseismic slip transients emerge spontaneously in three-dimensional rate and state modeling of subduction earthquake sequences. *Journal of Geophysical Research: Solid Earth*, *110*, B08307. https://doi.org/10.1029/2004JB003424

Liu, Y., & Rice, J. R. (2007). Spontaneous and triggered aseismic deformation transients in a subduction fault model. *Journal of Geophysical Research*, *112*, B09404. https://doi.org/10.1029/2007JB004930

McGuire, J. J., & Segall, P. (2003). Imaging of aseismic fault slip transients recorded by dense geodetic networks. *Geophysical Journal International*, *155*(3), 778–788.

Nishimura, T., Matsuzawa, T., & Obara, K. (2013). Detection of short-term slow slip events along the Nankai Trough, southwest Japan, using GNSS data. *Journal of Geophysical Research: Solid Earth*, *118*, 3112–3125. https://doi.org/10.1002/jgrb.50222

Nocquet, J., Villegas-Lanza, J., Chlieh, M., Mothes, P., Rolandone, F, Jarrin, P., et al. (2014). Motion of continental slivers and creeping subduction in the northern Andes. *Nature Geoscience*, *7*(4), 287–291.

Obara, K. (2002). Nonvolcanic deep tremor associated with subduction in southwest Japan. *Science*, *296*(5573), 1679–1681.

Obara, K. (2011). Characteristics and interactions between non-volcanic tremor and related slow earthquakes in the Nankai subduction zone, southwest Japan. *Journal of Geodynamics*, *52*(3), 229–248.

Obara, K., Hirose, H., Yamamizu, F., & Kasahara, K. (2004). Episodic slow slip events accompanied by non-volcanic tremors in southwest Japan subduction zone. *Geophysical Research Letters*, *31*, L23602. https://doi.org/10.1029/2004GL020848

Obara, K., & Kato, A. (2016). Connecting slow earthquakes to huge earthquakes. *Science*, *353*(6296), 253–257.

Obara, K., & Sekine, S. (2009). Characteristic activity and migration of episodic tremor and slow-slip events in central Japan. *Earth, planets and space*, *61*(7), 853–862.

Ohta, Y., Freymueller, J. T., Hreinsdóttir, S., & Suito, H. (2006). A large slow slip event and the depth of the seismogenic zone in the south central Alaska subduction zone. *Earth and Planetary Science Letters*, *247*(1-2), 108–116.

Peterson, C. L., & Christensen, D. H. (2009). Possible relationship between nonvolcanic tremor and the 1998–2001 slow slip event, south central Alaska. *Journal of Geophysical Research*, *114*, B06302. https://doi.org/10.1029/2008JB006096

Radiguet, M., Cotton, F., Vergnolle, M., Campillo, M., Valette, B., Kostoglodov, V., & Cotte, N. (2011). Spatial and temporal evolution of a long term slow slip event: The 2006 Guerrero Slow Slip Event. *Geophysical Journal International*, *184*(2), 816–828.

Rogers, G., & Dragert, H. (2003). Episodic tremor and slip on the Cascadia subduction zone: The chatter of silent slip. *Science*, *300*(5627), 1942–1943.

Rondenay, S., Montési, L. G., & Abers, G. A. (2010). New geophysical insight into the origin of the Denali volcanic gap. *Geophysical Journal International*, *182*(2), 613–630.

Rousset, B., Campillo, M., Lasserre, C., Frank, W. B., Cotte, N., Walpersdorf, A., et al. (2017). A geodetic matched filter search for slow slip with application to the Mexico subduction zone. *Journal of Geophysical Research: Solid Earth*, *122*, 10,498–10,514. https://doi.org/10.1002/2017JB014448

Rousset, B., Lasserre, C., Cubas, N., Graham, S., Radiguet, M., DeMets, C., et al. (2016). Lateral variations of interplate coupling along the Mexican subduction interface: Relationships with long-term morphology and fault zone mechanical properties. *Pure and Applied Geophysics*, *173*(10–11), 3467–3486.

Schwartz, S. Y., & Rokosky, J. M. (2007). Slow slip events and seismic tremor at circum-Pacific subduction zones. *Reviews of Geophysics*, *45*, RG3004. https://doi.org/10.1029/2006RG000208

Segall, P., & Matthews, M. (1997). Time dependent inversion of geodetic data. *Journal of Geophysical Research*, *102*(B10), 22391–22409.

Segall, P., Rubin, A. M., Bradley, A. M., & Rice, J. R. (2010). Dilatant strengthening as a mechanism for slow slip events. *Journal of Geophysical Research*, *115*, B12305. https://doi.org/10.1029/2010JB007449

Sekine, S., Hirose, H., & Obara, K. (2010). Along-strike variations in short-term slow slip events in the southwest Japan subduction zone. *Journal of Geophysical Research*, *115*, B00A27. https://doi.org/10.1029/2008JB006059

Shelly, D. R., Beroza, G. C., & Ide, S. (2007). Non-volcanic tremor and low-frequency earthquake swarms. *Nature*, *446*(7133), 305.

Shelly, D. R., Beroza, G. C., Ide, S., & Nakamula, S. (2006). Low-frequency earthquakes in Shikoku, Japan, and their relationship to episodic tremor and slip. *Nature*, *442*(7099), 188.

Takagi, R., Uchida, N., & Obara, K. (2019). Along-strike variation and migration of long-term slow slip events in the western Nankai subduction zone, Japan. *Journal of Geophysical Research: Solid Earth*, *124*, 3853–3880. https://doi.org/10.1029/2018JB016738

Tarantola, A. (2005). *Inverse problem theory and methods for model parameter estimation*. Philadelphia: Society for Industrial & Applied.

Thomas, A. L. (1993). Poly 3D: A three-dimensional, polygonal element, displacement discontinuity boundary element computer program with applications to fractures, faults, and cavities in the earth's crust (Master's Thesis), Stanford University.

Wallace, L. M., Beavan, J., Bannister, S., & Williams, C. (2012). Simultaneous long-term and short-term slow slip events at the Hikurangi subduction margin, New Zealand: Implications for processes that control slow slip event occurrence, duration, and migration. *Journal of Geophysical Research*, *117*, B11402. https://doi.org/10.1029/2012JB009489

Wech, A. G. (2016). Extending Alaska's plate boundary: Tectonic tremor generated by Yakutat subduction. *Geology*, *44*(7), 587–590.

Wech, A. G., & Bartlow, N. M. (2014). Slip rate and tremor genesis in Cascadia. *Geophysical Research Letters*, *41*, 392–398. https://doi.org/10.1002/2013GL058607

Wech, A. G., & Creager, K. C. (2011). A continuum of stress, strength and slip in the Cascadia subduction zone. *Nature Geoscience*, *4*(9), 624.

Wei, M., McGuire, J. J., & Richardson, E. (2012). A slow slip event in the south central Alaska Subduction Zone and related seismicity anomaly. *Geophysical Research Letters*, *39*, L15309. https://doi.org/10.1029/2012GL052351